Wireless Passive RFID Crack Width Sensor for Structural Health Monitoring

S. Caizzone, E. DiGiampaolo

***Abstract*—All mechanical structures are subject to deformation and cracks, due to fatigue, stress and/or environmental factors. It is therefore of uttermost importance to monitor the mechanical condition of critical structures, in order to prevent catastrophic failures, but also to minimize maintenance costs, i.e. avoid unnecessary inspections. A number of technologies and systems can be used for this purpose: among them, the ones proposing the use of wireless passive crackmeters have a strong impact potential, in terms of simplicity of installation and measurement and low cost. The present work hence shows a crack width wireless radio frequency identification (RFID) sensor, developed for applications on various materials (such as concrete and metal) and able to detect sub-millimeter deformations occurring on the object on which it is placed. A design method based on high sensitivity phase detection is shown.**

***Index Terms*—RFID, array, mutual coupling, sensors, wireless communications, SHM, crack monitoring**

I. Introduction

Structural health monitoring (SHM) systems [1] are automated tools, aimed at rapidly identifying the onset of structural damage and at tracking the condition of structures during forced or natural excitation. They resort to novel sensing technologies by combining extensive monitoring infrastructures with specific algorithms. With the increase in the demand for such systems and because of the large set of applications, the field of SHM has embraced a number of different technologies that differ in terms of complexity, measurement accuracy, life span and cost. A comprehensive review of the topic including physical monitoring principles, sensors, systems, signal processing and applications is shown in [2]. Regarding the used techniques, it is possible to distinguish among in-situ, on-demand and remote monitoring techniques. The first family is based on the deployment of several local sensors permanently coupled with structural elements: accelerometers, fiber optics, ultrasonic devices are some examples. The second family of techniques is based on instrumentation brought to the measurement site on-demand: X-ray, infrared thermography, laser scanning, microwave radar are the most common ones. Finally, the third family resorts to sensors far from the infrastructure site, such as those based on photogrammetry and interferometry techniques. To limit the discussion to the area of in-situ SHM systems, the available techniques can be divided into two groups, according to the use of wired or wireless technology.

Among the wired ones, high measuring precision and great resolution can be obtained, for instance, using fiber optic systems (e.g.[3][4]). However, such systems involve a time consuming installation, due, among others, to wiring problems; moreover, they are quite expensive, because of the complicated manufacturing as well as the extensive signal processing.

On the other hand, thanks to the fast and easy installation, wireless sensors are gaining a growing interest. A summary review is reported in [5]. In active wireless systems, each sensor node is typically battery-powered and permits a long distance transmission of the measured data. Although commercial solutions are appearing on the market, their cost and complexity is still relatively high and their autonomy limited by the lifespan of the battery (e.g. [6]).

Passive wireless systems, instead, harvest their energy from the environment or collect it from the powered read-out unit during the wireless communication: they have a simpler electronics and enable hence lower costs, at the expense of some sensor performance. Despite this reduction in obtainable performance, they appear as most appealing for the pervasiveness that their low cost could enable. In practice, a large deployment of such sensors can be used [7] as an *indicative monitoring ecosystem*, where passive sensors would provide initial information and detect criticalities with a low cost infrastructure spread out over the area to monitor: only the locations exhibiting problematic evolution of the monitored parameters would then be assessed with more precise (and expensive) technologies. This concept is for instance well suited for monitoring the evolution of already existing cracks (such as in historical buildings) or of junctions prone to cracks, similarly to what is often done with cheap visual crackmeters. In this case, a low-cost wireless passive sensor, able to detect sub-mm crack width variations with a dynamic range of a few mms, could become an enabler for a whole new set of indicative monitoring use cases.

A review of passive wireless sensors for SHM is reported in [8]. We will take into consideration only chip-less and RFID sensors here for brevity: they exploit the shift of resonance frequency of an antenna due to a modification of the antenna geometry or the underlying substrate because of a mechanical stress. Rectangular [9] and circular [10] microstrip patch antennas have been used in chip-less systems: they exploit the change of the resonant frequency due to the change of the characteristic dimensions of the antenna, provoked by the strain applied on the antenna, and record it wirelessly by means of a second antenna connected to a vector network

S. Caizzone is with the Institute of Communications and Navigation, German Aerospace Center (DLR), Oberpfaffenhofen, Germany, as well as with the DISP, University of Roma Tor Vergata, Italy. E-mail: stefano.caizzone@dlr.de.

E. DiGiampaolo is with the Dipartimento di Ingegneria Industriale e dell'Informazione e Economia, University of L'Aquila, Italy. E-mail: emidio.digiampaolo@univaq.it.

analyzer (VNA). The read distance is in general short (i.e. tens of centimeters) while the measurement accuracy can be good. A small microresonator structure that generates an amplitude peak in the radar cross-section at resonance is instead proposed in [11]. The frequency-domain backscatter signature of the resonator includes its ID and the measured value. The transduction of the strain information into the signal is obtained by a variation of the capacitive element of the resonator along with the measured quantity. Sub millimeter measurement accuracy is achieved, but a large frequency band is used and a spectrum analyzer is required. The operating distance is below 1m. Another interesting solution is proposed in [12], where a two-element antenna array is placed on the two sides of the crack and the evolution of the latter is monitored by exploiting the changes in array radiation characteristics when the distance between the elements changes. However, the system is not standardized and requires a precise measurement readout, with expensive equipment.

The previous examples have the drawback of high costs and/or complicated measurement read-out. On the other hand, RFID sensors could help in overwhelming such issues, thanks to their ease of installation and wireless readout. Moreover, the use of a fully standardized identification technology (ultrahigh frequency (UHF) RFID EPC1Gen 2) has the benefit of low cost of commercial off the shelf (COTS) components. A few passive RFID designs have been proposed in recent literature to serve as deformation/crack sensors. They all exploit detuning of the tag due to deformation of the structure. A metal plate is used in [14] to detune an RFID tag applied on a beam as it gets deformed. Deformation is measured by monitoring the tag backscatter signal strength and the minimum turn on power. A rectangular microstrip patch antennas in combination with IC chips is proposed in [15], forming an RFID strain sensor whose resonant frequency changes along with change in its dimension due to strain. A meander dipole antenna is used in [16] as a strain sensor exploiting the change of the turn-on power in consequence of the detuning due to the stretching of the meander. Detuning based sensors however sacrifice read range for the sake of sensing: the read range reduction, due to tag detuning, can also be of the order of 10 dB. In [17], instead, the authors have demonstrated that phase information from RFID tags can be usefully exploited to infer deformation of ad-hoc designed couplet of RFID tags, only weakly affecting the read range. The coupling between two (dipole) antennas is in that case exploited, somehow similarly to the concept proposed in [12], but allowing here for compensation of the varying self-impedance through the mutual impedance. A comparison of the different system approaches, with a summary of achievable performance and required setup, is shown in Tab. I.

The present work, taking cue from [17], explores how to adapt and optimize the design of RFID passive sensors for crack monitoring in environments considered to be RFID-harsh, either because of relatively high dielectric losses (like in concrete) or because of the presence of metallic materials.

Passive RFID sensors do in fact depend on the surrounding environment, because they rely on wireless measurement of antenna-related parameters.

Dipoles, for instance, as the ones used in [17], are not suitable for this kind of applications because of their reknown dependence on the underneath material. On the other hand, microstrip patch antennas, thanks to their ground plane, are substantially less influenced by the underlying materials than dipole-type antennas: in fact, the ground plane helps in insulating the antenna from what is underneath, effectively making the antenna almost insensitive to the underlying material. For the former reasons, a microstrip antenna has been considered in this work: the miniaturized planar-inverted-F antenna (PIFA) proposed in [18] (with a realized gain around -8 dBi) served as starting point for the present investigation.

System typology	Relevant parameters	Performance		Measurement set-up
		Resolution	Read Range	
Chip-less	resonant frequency [9],[10],[11]	sub-mm	<1 m	complex (VNA-based)
	null-pattern position [12]	few mm	>>1m	complex
RFID detuning-based	backscattered power [14]	few mm	~1 m	specific equipment
	turn-on power [15]	sub-mm		
	turn-on power [16]	sub-mm		simple (COTS-based)
RFID phase-based	phase of backscattered signal ([17] and present work)	sub-mm	>1 m	simple (COTS-based)

Table I
COMPARISON OF DIFFERENT TECHNOLOGIES FOR CRACK WIDTH ENLARGEMENT DETECTION IN SHM APPLICATIONS

A proper design for the adequate antenna typology in couplet configuration will be shown in this work, enabling the sensor to gain in terms of applicability on various materials and releasing it from the need for in situ structure-dependent calibration. The size of the tag antenna (including also the ground plane) is moreover an issue, with miniaturized solutions being preferred because of minor obstruction concerns in real-life structures as well as of the inherently local nature of crack measurement. However, miniaturized antennas are more strongly influenced by the surrounding environment, as their fields are not totally confined, but extend to nearby objects.

A proper trade-off between miniaturization and material independence is found in Sec. II.C.

The paper is divided as follows: the theoretical background and the design approach will be shown in Sec. II, while measurements of the prototype are presented in Sec. III. Finally, conclusions are drawn in Sec. IV.

II. THEORY AND DESIGN METHOD

A. Theoretical Background

The envisaged system is shown in Fig. 1: it is composed of an RFID reader, wirelessly interrogating a couplet of RFID tags, each placed on one edge of a crack on the surface of the structure to monitor.

If two close RFID tags, strongly coupled with each other, are considered, it is possible to achieve a good variation of the phase of the backscattered field with respect to variation

of their mutual distance [17], hence having the chance to turn the RFID couplet into a deformation sensor.

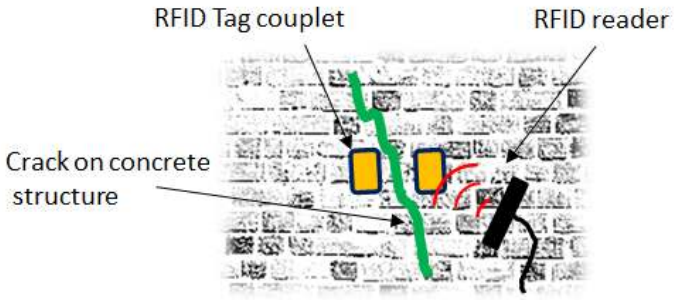

Figure 1. Envisaged system layout: an RFID reader wirelessly interrogates a couplet of RFID tags placed on a cracked wall-like structure and retrieves deformation data

However, particular care has to be taken in order to limit the variation of the useful read range of the tags during the sensing process: as a matter of fact, coupling as well as detuning can worsen the power requirements of tags (i.e. tags could be readable only from a shorter distance). To avoid the shortening of the communication distance, a trade-off analysis between the communication (i.e. read range) and sensing (i.e. deformation) requirements shall be implemented. The final aim of the design is to develop a sensor with good phase (and hence crack width) sensitivity and, at the same time, no drastic variation in communication capabilities (i.e. read range) along the sensing process.

For what concerns sensing, the phase of the tag n ($n = 1, 2$) of a couplet of symmetric tags can be expressed [17] as

$$\varphi_n[d] = \varphi_Z + \varphi_0 = \tag{1}$$

$$= arg\left\{-\frac{Z_S[d] - Z_M[d] + Z_C}{(Z_S[d] + Z_C)\,(Z_S[d] + Z_M[d] + Z_C)}\right\} + \varphi_0$$

where Z_S is the self impedance of one tag, Z_M is the mutual impedance, Z_C the chip scavenging impedance and d is the mutual distance between the tags.

φ_0 is defined as $\varphi_0 = arg\{f(r_n)\} = \varphi_r + \varphi_h$, where

$$f(r_n) \propto \frac{\lambda^2}{\pi^2}\sqrt{P_{in}R_R^{rad}/2}G_R R_n^{rad} G_n^{OC}(\hat{\underline{h}}_n \cdot \hat{\underline{h}}_R)^2 \frac{e^{-j2kr_n}}{4r_n^2} \tag{2}$$

and where λ is the wavelength, P_{in} is the power supplied by the reader, R_R^{rad} and $R_n^{rad}[d]$ are, respectively, the radiation resistance of the reader and of the n-th tag antenna, G_R is the gain of the reader antenna, $G_n^{OC}[d]$ the gain of the n-th tag (when the other tag is in open circuit condition), $\hat{\underline{h}}_R$ and $\hat{\underline{h}}_n[d]$ are respectively the effective height unitary vector of the reader and of the n-th tag antenna.

The phase of the tag is thus composed of three parts:

$$\varphi_n = \varphi_Z + \varphi_0 = \varphi_Z + \varphi_r + \varphi_h \tag{3}$$

The first one (φ_Z) depends only from the impedance matrix and the chip impedance (being the first term of Eq. 1); the second one ($\varphi_r = -2kr_n$) is determined by the reader-tags distance and the third one from the phase of the product of effective heights of reader and tag ($\varphi_h = arg\{(\hat{\underline{h}}_n \cdot \hat{\underline{h}}_R)^2\}$). It will here be assumed that the *measurement setup is fixed*, meaning that the distance and orientation between reader and tags do not change for subsequent measurements. Considering that the distance d between the tags has a range of few mm, corresponding to hundredths of λ, we can assume that the effective height of the tag will not change strongly in the range of d. Therefore, φ_r and φ_h can be assumed constant with the crack evolution and therefore the phase change will only be due to φ_Z .

Communication properties on the other hand depend mainly on the power transmission coefficient τ_n and realized gain $\widetilde{G}_n$, which influence the power scavenging capability, and the modulation efficiency ME_n, that affects the capability of correct demodulation of the signal backscattered from the nth tag to the reader [20]. Both parameters can be optimized as functions of the self and mutual impedances, obtaining different trade-offs in terms of τ_n and ME_n.

The power scavenging capability, maximized around the Hermite condition $Z_{in,n} = Z_{chip}^*$, is usually expressed in terms of power transmission coefficient [17]:

$$\tau_n[d] = \frac{4R_C R_S^{rad}[d]}{|Z_{in,n}[d] + Z_C|^2} \tag{4}$$

whereR_S^{rad} and R_C are respectively the self radiation resistance and chip resistance, while $Z_{in,n}$ is the input impedance, and realized gain

$$\widetilde{G}_n[d] = G_n^{OC}[d]\tau_n[d]\chi_n \tag{5}$$

with $\chi_n = \left|\hat{\underline{h}}_n \cdot \hat{\underline{h}}_R\right|^2$ being the polarization mismatch coefficient.

The modulation efficiency ME shall instead be maximized for optimizing the modulated backscattered power and can be written as [20]

$$ME_n[d] = \frac{4R_{in,n}^2[d]\left|[Z_C^{OFF} - Z_C^{ON}\right|^2}{\left|Z_{in,n} + Z_C^{ON}\right|^2\left|Z_{in,n} + Z_C^{OFF}\right|^2} \tag{6}$$

thus with a clear dependence on both the modulation impedances of the RFID chip, Z_C^{ON} and ${Z_C}^{OFF}$, and on $Z_{in,n}$. The modulation efficiency is particularly important in the case of up-link limited systems. In the case of down-link limited systems, e.g. for typical passive systems as well as for the solution presented in this work, it is instead essential to optimize the scavenged power required for turning on the chip. It is worth recalling that also passive systems can be up-link limited, for instance when the latest top performing RFID chips, with their constant improvement in terms of sensitivity, are used, together with simple (and not extremely sensitive) readers: in such case, the modulation efficiency shall be considered as the parameter to optimize, implying the need for measuring the actual values of both impedance states of the chip [21]. In our case, however, by performing a power budget calculation [22] with the used NXP G2XM chip, the system has been proven down-link limited and therefore the

realized gain, incorporating all the necessary phenomena (i.e. impedance matching through τ_n, polarization mismatch χ_n, antenna gain G_n^{OC}), will be in the following the parameter to optimize for the communication capability.

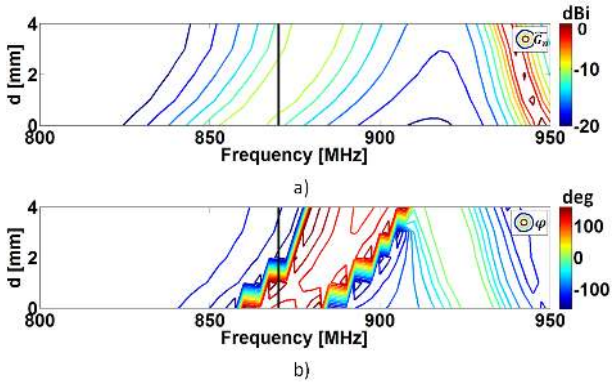

Figure 2. Isolines of: a) realized gain; b) phase over mutual distance and frequency for a couplet of PIFA antennas

Fig. 2 shows $\widetilde{G}_n$ and φ_n of one tag of a couplet of PIFA antennas (see Fig. 3) versus frequency and mutual distance, giving a rationale for the use of (the phase of) coupled tags for deformation monitoring.

It can in fact be seen that in a particular area of the graph (marked by the black vertical line and corresponding to a specific working frequency), $\widetilde{G}_n$ has few variations, implying minimal degradation of communication performance (i.e. $\widetilde{G}_n$ is almost constant), while phase is strongly varying with mutual distance, especially in the first millimeters. Operation in a zone with such properties could therefore be particularly suitable to satisfy both requirements on communication and sensing, which, on the other hand, would not be satisfied at the same time in other regions of the plot.

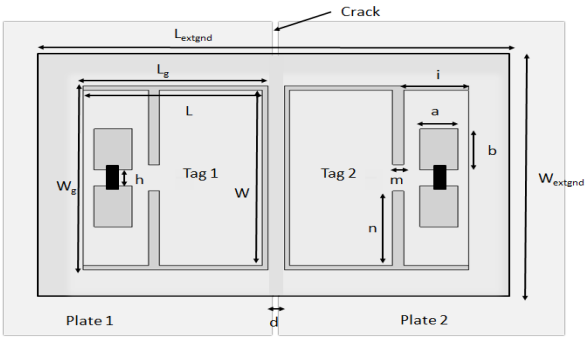

Figure 3. Proposed crack width sensor, composed of two RFID tags placed each on one edge of a cracked structure (top view). Each tag consists of a PIFA antenna. Relevant design parameters are shown

B. Design Procedure

The performance of the sensor (in terms of phase and realized gain variations) can be optimized by means of an appropriate choice of the design parameters of the antenna couplet, which then become degrees of freedom (DOFs) for the optimization process. The design parameters that mainly affect the tuning of the chosen antenna (Fig. 3) are a (the width of the H-slot) and n (the slit length).

It is therefore possible to optimize the performance of the RFID couplet, choosing n and a as DOFs and $\triangle\varphi_{min}$ and $\widetilde{G}_{nmin}$ as requirements.

The optimization constraints can be formally expressed as

$$\begin{cases} \varphi_n(d_{max}) - \varphi_n(d_{min}) \geq \Delta\varphi_{n,min} \\ \widetilde{G_n}(d) \geq \widetilde{G}_{n,min} \end{cases} \quad (7)$$

$$\forall n,\ \forall d\epsilon[d_{min}; d_{max}]$$

In other words, only configurations (i.e. given values of a and n) of the antennas satisfying simultaneously requirements on minimal variation of phase and minimal realized gain along the whole process (i.e. for the whole interval of distances) can be accepted for the final design.

In the optimization process, we choose the following requirements for communication and sensing $\widetilde{G}_{n,min} = -16\ dBi$ and $\Delta\varphi_{n,min} = 80\ °$ with a range of distances $[d_{min};\ d_{max}] = [1;\ 3]$ mm. The choice of the minimum value of realized gain is related to the specific kind of antenna adopted: in this case, the miniaturization of the single antenna (as shown in [18]) as well as the additional losses due to coupling do not allow for high gain values. However, $\widetilde{G}_{n,min} = -16\,dBi$ still seems a reasonable value, as it guarantees a read range of around 1.5 m for an equivalent isotropic radiated power (EIRP) of 3.2 W and with the used microchip (i.e. a NXP G2XM with a sensitivity $p_{c,n}$ of -15 dBm), which is large enough for the proposed application. Even better read ranges can be obtained if using more performing chips, i.e. chips with lower sensitivities. The choice of the minimum value of the phase difference $\Delta\varphi_{n,min}$ originates from the desired sensitivity of the couplet, i.e. the desired variation of the phase over a given interval of distance. $\Delta\varphi_{n,min}$ shall be high enough to easily distinguish the phase variation due to the crack enlargement, with respect to the phase resolution of the reader. Higher values will thus enable finer crack width resolutions. On the other hand, if the requested $\Delta\varphi_{n,min}$ is too high, the optimization process might not converge. A balanced value has hence been chosen, enabling to clearly distinguish sub-mm displacements.

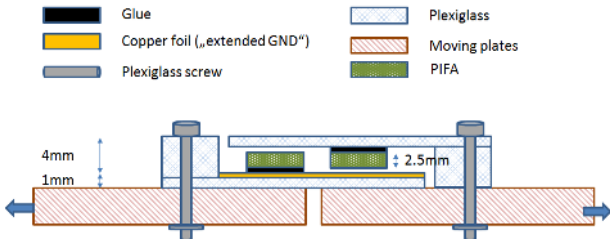

Figure 4. Proposed deformation sensor (side view). The sliding plexiglass structure is mutuated from visual crackmeters

In order to ensure maximal applicability of the sensor on areas made of different materials (for instance, the concrete blocks of buildings as well as metallic plates of an avionic

part), the two RFID tags have been equipped with a Plexiglas sliding support (Fig. 4), that ensures a similar and controlled relative positioning and sliding of the tags on every structure they might be placed on. In the present work, only a sliding of the tags along the direction that connects one tag to the other will be considered, i.e. only an enlargement of the crack width will be taken into account.

Due to the fact that the used antennas are miniaturized, they are not totally able to confine the fringing field produced at the edges of the PIFA antennas. The use of an additional and larger layer of copper below the tags may help therefore in reducing the field interacting with underlying materials, improving the tags' invariance from the structure below. For such reason, the upper surface of the lower horizontal Plexiglas sheet is fully covered with a thin copper foil (referred to as "extended ground"). The width of the copper sheet (and of the Plexiglas) has at first been assumed as relatively big (W_{extgnd}= 200 mm), in order to ensure isolation from the underlying material: this dimension can of course be diminished if the specific application requires a smaller lateral footprint, however with the disadvantage of a decreased independence from the underlying material, as shown in Sec. II.C.

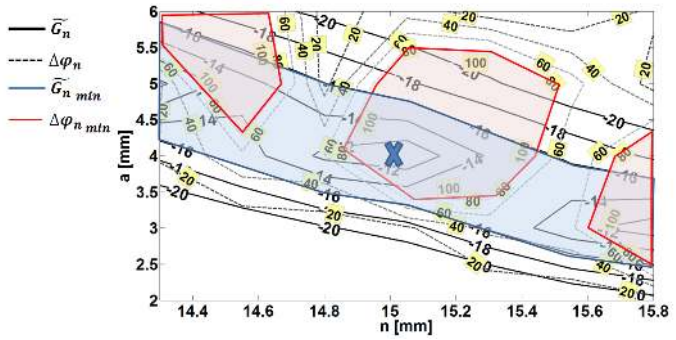

Figure 5. $\triangle\varphi$ vs. $\widetilde{G}_n$ chart for two strongly-coupled PIFA antennas placed over two concrete plates (as in Fig. 12) with n and a as degrees of freedom. Blue and red areas highlight regions of the parameters domain where optimal performance, in terms of communication and sensing, are obtained.

Considering the requirements expressed above and having assumed that the sensor, comprising the couplet of tags and the Plexiglas support, is fixed on two adjacent concrete plates (with dimensions $50x25x10$ cm) and that a NXP G2XM chip is used (with $Zc = 15 - j135\,\Omega$ at $f_{RFID} = 867\,MHz$), the resulting $\triangle\varphi$ and $\widetilde{G_n}$ chart is plotted in Fig. 5.

Considering the intersection of admissible regions for communication and sensing, shown respectively as blue and red areas in Fig. 5, optimal results are found for $n = 15.0\,mm$ and $a = 4.2\,mm$.

The phase and realized gain variation with respect to mutual distance for the optimal result are plotted in Fig. 6: a strong variation of phase in the whole range $[d_{min};\ d_{max}] = [1;\ 3]$ mm can be seen, as opposed to limited variations of $\widetilde{G}_n$, thus in compliance to the trade-off guidelines.

The obtained optimization results permit to evaluate better the effects of the target values chosen for $\triangle\varphi_{min}$ and $\widetilde{G}_{nmin}$. By imposing a $\triangle\varphi_{min} = 80\,°$, we ensure a good crack width detection capability. As a matter of fact, with such requirement and due to the phase resolution of 3 ° available in many low-cost commercial RFID readers, about 30 different crack width levels can be theoretically measured in the dynamic range $[d_{min};\ d_{max}]$: this results in a theoretical crack width resolution $\partial d < 0.1\ mm$, therefore abundantly satisfying the sub-mm resolution requirement.

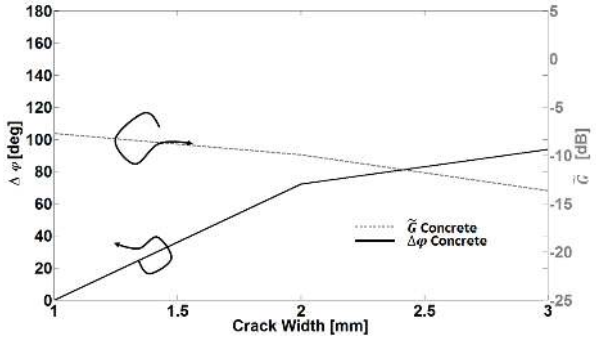

Figure 6. $\widetilde{G}$ and $\Delta\varphi$ variations as the crack enlarges, when the sensor is placed over two concrete plates. Dimensions of the PIFA [mm]:$W_g = 45$, $L_g = 34$, $W = 43$, $L = 33$, $i = 12$, $m = 2$, $n = 15.05$, $b = 10$, $a = 4.2$, $h = 4$, $W_{extgnd} = 200$

On the other hand, the imposed constraint on communication is not too stringent, in order to facilitate the optimization convergence: some realized gain variations are visible in the sensor dynamic range (i.e. about 3.5 dB difference between maximum and minimum gain during the sensing process), but they do not prevent from satisfying the realized gain requirement in the whole dynamic range of the sensor.

Of course, different constraints can be imposed during the optimization process, if requested by the application, for instance choosing a higher minimum realized gain.

Thanks to the relatively large copper sheet used (i.e. $W_{extgnd} = 200$ mm), the behaviour of the sensor impedance (and hence of phase and realized gain) is proven similar on various materials, such as metallic or wooden plates (Fig. 7).

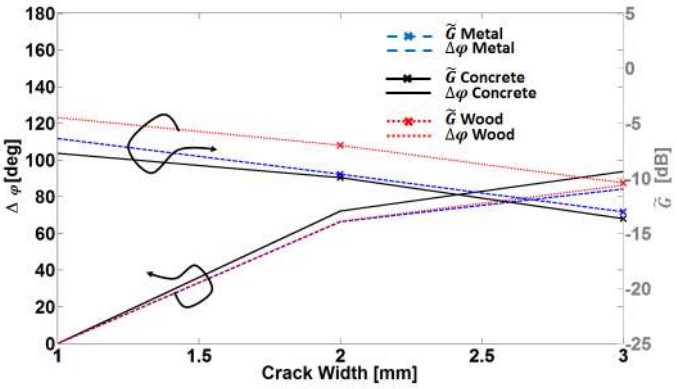

Figure 7. $\widetilde{G}$ and $\Delta\varphi$ variations as the crack enlarges, when the sensor is placed over two plates made of wood, metal or concrete. $W_{extgnd} = 200$ mm.

A slightly higher realized gain is observed for the wood configuration, most probably due to the different absorbing/scattering properties of wood with respect to the residual

fields at the edge of the extended ground plane (see Sec. II.C). This results however simply in a better communication capability for the sensor when placed on wood. No phase variation is instead recorded when placing the sensor on different materials, hence enforcing the suitability of this design for use on different materials.

The design procedure can therefore be summarized in the following steps:

- Identify the range of crack widths of interest, i.e. $[d_{min};\ d_{max}]$, the required measurement resolution ∂d and the minimum read range r
- Derive requirements on $\Delta\varphi_{n,min}$ and $\widetilde{G}_{n,min}$ from the previous specifications. In particular:
  - $\Delta\varphi_{n,min} > \frac{\partial\varphi}{\partial d}(d_{max} - d_{min})$, with $\partial\varphi$ the phase resolution of the reader and ∂d the required sensor resolution;
  - $\widetilde{G}_{n,min} = \frac{p_{c,n}}{\left(\frac{\lambda}{4\pi r}\right)^2 P_{in} G_R \chi_n}$ with $p_{c,n}$ being the chip sensitivity and G_R the gain of the reader antenna.
- Optimize the antenna layout until the requirements are satisfied, e.g. by means of an electromagnetic (e.m.) solver.

C. Effects of Ground Plane Miniaturization

For many applications, the size of the sensor is crucial for its applicability. Therefore, the width of the extended ground should be the minimal one able to maintain the capability of the sensor to be independent from the underlying materials. Fig. 8 shows the electric field distribution over the additional ground plane for different W_{extgnd}: as the width decreases, stronger electric fields accumulate along the lateral edges of the extended ground plane and then interact with the underlying material (and re-radiate): this causes a stronger dependence of the response of the sensor on underlying materials.

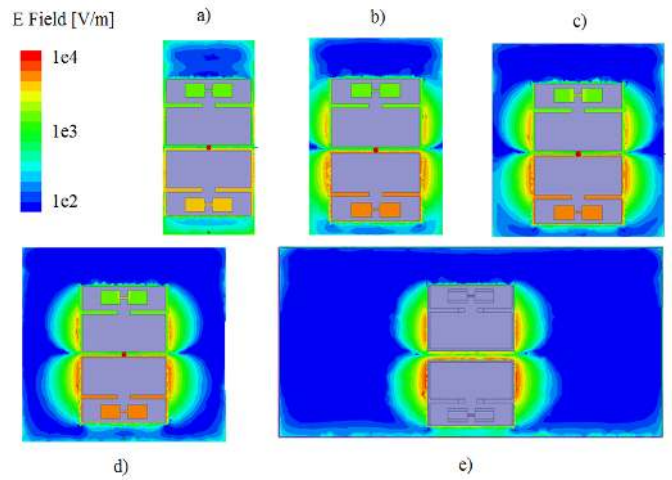

Figure 8. Electric field distribution on extended ground plane for different ground widths (Pictures a)-e) respectively: W_{extgnd}=47, 65, 85, 100, 200 mm). The progressively diminishing field on the edges of the copper sheet explains the improved independence from the underlying material

On the other hand, for bigger widths of the extended ground plane, the electric field on the lateral edges of the ground is noticeably reduced and hence the antenna exhibits a strongly improved independence from the underlying environment.

At W_{extgnd}= 100 mm, the sensor response (Fig. 9), both in terms of phase and $\widetilde{G}_n$, is still very similar to the one considered before (Fig. 7) for all tested materials.

For smaller widths, on the other hand, (e.g. W_{extgnd}= 47 mm as in Fig. 10) the behaviour of the phase is noticeably different on each material.

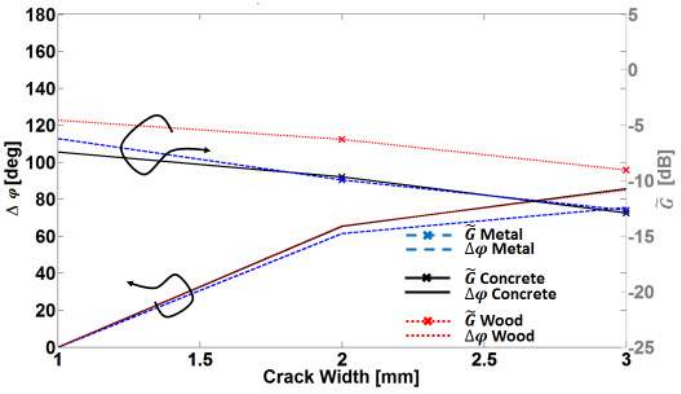

Figure 9. $\tilde{G}$ and $\Delta\varphi$ variations as the crack enlarges, when the sensor is placed over two plates made of wood, metal or concrete and the Plexiglas support (and hence the extended ground plane) has a width of 100 mm

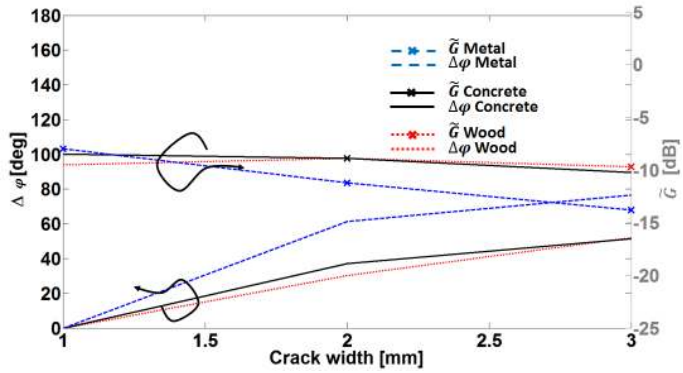

Figure 10. τ and $\Delta\varphi$ variations as the crack enlarges, when the sensor is placed over two plates made of wood, metal or concrete and the Plexiglas support (and hence the extended ground plane) has a width of 47 mm

As a matter of fact, if miniaturization of the lateral side of the sensor is requested, W_{extgnd}= 100 mm can be considered as the minimum size to maintain similar operation on any structure. If smaller sizes are required, an ad-hoc calibration procedure shall be performed for every different installation setup, to take into account the interaction of the sensor with the actual materials of the structure.

III. Measurement Results

The simulated design has been manufactured, in order to perform crack width enlargement tests (Fig.11). After being integrated with the plexiglass support, the prototype has been placed over two neighboring concrete plates to test its performance in real life conditions (Fig. 12) . In order to simulate the crack growth, one plate has been progressively moved away

from the other by using a precise translation mechanism. As the block was moved, the crack enlargened, as in Fig. 12.

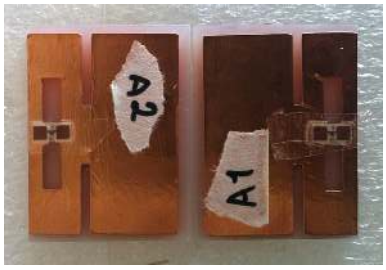

Figure 11. Manufactured prototypes: antennas without support

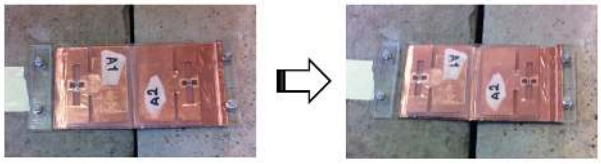

Figure 12. Manufactured prototypes: sensor mounted on concrete plates as the distance between the plates (representing the crack) enlarges

The measured phase and realized gain are shown in Fig. 13, at $f_{RFID} = 867\,MHz$. Measurements are done through a Thingmagic M6e low-cost reader [23]. Phase, RSSI (Received Signal Strength) and turn on power (i.e. the minimum power at reader's antenna terminals necessary to weak up the tag) are measured at each crack width: from turn on measurement (P_{TO}), it is then possible to estimate realized gain [24], by using the following equation

$$\widetilde{G}_n = \frac{p_{c,n}}{\left(\frac{\lambda}{4\pi r}\right)^2 P_{TO} G_R \chi_n} \tag{8}$$

The measurement is repeated 30 times per crack width, in order to calculate an average value, less affected by noise, for the phase information. Such procedure helps in obtaining more accurate results: on the other hand, thanks to the fast interrogation rate of modern RFID systems, only a few seconds are needed for a set of 30 measurements, hence still being acceptable for almost real-time operation. Error bars in Fig. 13 represent the measured standard deviation of phase along each set of 30 measurements.

The same measurement procedure has been performed with plates of different materials, i.e. concrete, wood and metal, to test the sensor usability on all structures.

Both phase variation and realized gain profiles are aligned with the simulated results and show good agreement: in particular, a phase variation of around 100 degrees in 2 mm is observable for all materials, meaning that a resolution of less than 0.1 mm can be theoretically obtained (by considering that the phase resolution is around 3° for the low cost Thingmagic M6e reader).

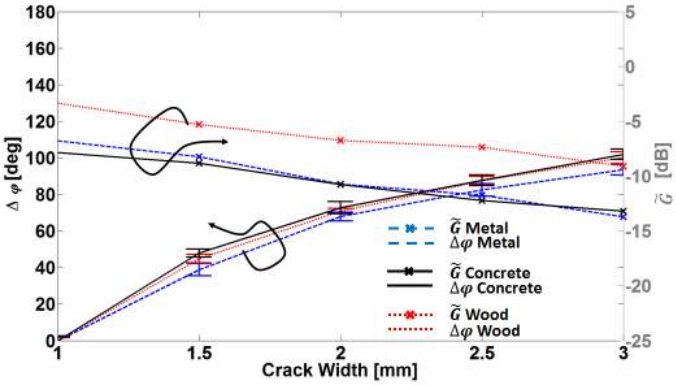

Figure 13. Measured $\widetilde{G}$ and $\Delta\varphi$ variations as the crack enlarges, when the sensor is placed, respectively, over: two concrete plates, two wooden plates, two metallic plates. Extended ground plane width: 100 mm

Some noise oscillations in phase measurement, due to the fact that the measurements have been performed in a real laboratory environment, with no attempt to mitigate multipath or reflections from nearby objects, increase however the standard deviation of the measures and therefore a minimum detectable crack enlargement of 0.2 mm can be precautionary assumed.

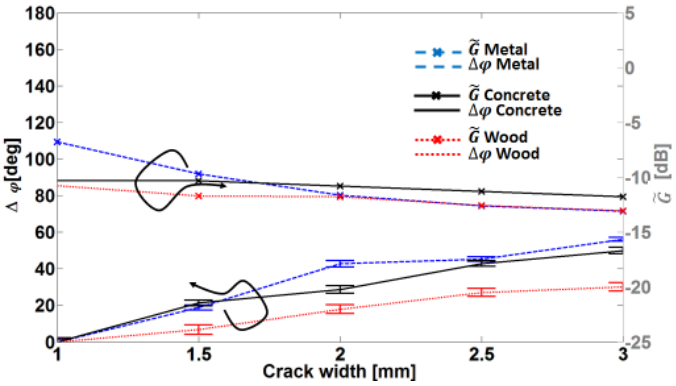

Figure 14. Measured $\tilde{G}$ and $\Delta\varphi$ variations as the crack enlarges, when the sensor is placed over two plates made of wood, metal or concrete and the extended ground has a width of 47 mm

In the analysed sensing range, a realized gain higher than -15 dBi is observable for all materials, meaning that the sensor can still be read from a distance of 1.5 m (at EIRP=3.2 W and with a chip sensitivity of -15 dBm), as expressed in the requirements and very similarly to simulation results. Also measurements with smaller W_{extgnd} have been performed (Fig. 14): although phase variations are visible also in this case, different behaviours can be observed for the various materials, proving the reduced material independence due to a smaller extended ground plane, as explained in Sec. II.

The measured results show therefore the real life applicability of the proposed sensor. Tests on different materials (concrete, metal, wood) validated its reproducible behaviour on different objects to be monitored and thus its suitability for application as sub-mm crack enlargement detector for indicative monitoring in RFID harsh environments.

IV. Conclusion

The possibility to monitor crack progression on concrete structures by means of a passive RFID based wireless sensor system has been here demonstrated and validated, both by simulation and laboratory measurement. A trade-off between communication capabilities and crack enlargement sensitivity has been shown by means of a parametric design method, enabling good sensing with limited communication degradation. Good agreement between simulated and measured results is found when the sensor is placed on concrete structures, as well as on various other materials, proving that the proposed sensor is usable as a generic wireless crack meter. Different applications are foreseeable, such as monitoring of concrete walls in ancient buildings or metallic frameworks in bridges or aeronautic structures. The proposed system is designed for 1D crack enlargement: more complicated structures, able to slide on two orthogonal planes, can be also foreseen.

Due to the use of phase as sensing parameter, some measurement precautions have been adopted: on the one hand, multiple measurement samples for each crack width diminish the effects of spurious noise on phase and hence help in achieving more accurate read-outs, without nevertheless impacting drastically on the total measuring time, i.e. allowing for almost real-time measurement. On the other hand, the system is dependent on the distance between reader and tags and therefore a fixed measurement setup was employed, so that the distance and orientation between reader and tags do not vary all along the sensing process. Such constraint is however not limiting in many test environments, where the monitoring infrastructure can be considered fixed. A setup independent phase parameter is an open issue for further research, already being tackled by the authors.

References

[1] P.C. Chang, A. Flatau, S.C. Liu, “Review paper: health monitoring of civil infrastructure”, *Structural Health Monitoring*, vol. 2, no. 3, pp. 257-267, Sept. 2003

[2] *Encyclopedia of Structural Health Monitoring*, John Wiley and Sons, Inc., 2014 DOI: 10.1002/9780470061626

[3] F. Ravet, F. Briffod, B. Glisic, M. Nikles, D. Inaudi, "Submillimeter crack detection with Brillouin-based fiber-optic sensors", *IEEE Sensors J.*, vol. 9, no. 11, pp. 1391-1397, Nov. 2009

[4] M. Ramakrishnan, G. Rajan, Y. Semenova, G. Farrell, "Hybrid fiber optic sensor system for measuring the strain, temperature and thermal strain of composite materials", *IEEE Sensors J.*, vol. 14, no. 8, pp. 2571-2578, Aug. 2014

[5] J. P. Lynch, K. J. Loh, “A summary review of wireless sensors and sensor networks for structural health monitoring”, *Shock Vib. Dig.,* vol. 38, pp. 91–128, 2006.

[6] A. Ledeczi, T. Hay, P. Volgyesi, D. R. Hay, A. Nadas, S. Jayaraman, "Wireless acoustic emission sensor network for structural monitoring", *IEEE Sensors J.*, vol. 9, no. 11, pp. 1370-1377, Nov. 2009

[7] P. Kalansuriya, R. Bhattacharyya, S. Sarma, "RFID tag antenna-based sensing for pervasive surface crack detection", *IEEE Sensors J.*, vol. 13, no. 5, pp. 1564-1570, May 2013

[8] A. Deivasigamani, A. Daliri, C. Wang, and S. John, ’A review of passive wireless sensors for structural health monitoring’, *Modern Applied Science*, vol. 7, no. 2, pp. 57-76, 2013

[9] S. Deshmukh, H. Huang,”Wireless interrogation of passive antenna sensors”, *Measurement Science and Technology*, 21, 035201, 2010

[10] A. Daliri, A. Galehdar, S. John, C.H. Wang, W.S.T. Rowe, K. Ghorbani, “Wireless strain measurement using circular microstrip patch antennas”, Sensors and Actuators A: Physical, 184, 86-92, 2012

[11] C. Mandel, M. Schussler, R. Jakoby, "A wireless passive strain sensor," IEEE Sensors, vol., no., pp.207,210, 28-31 Oct. 2011

[12] V. Rizzoli, A. Costanzo, E. Montanari, A. Benedetti, "A new wireless displacement sensor based on reverse design of microwave and millimeter wave antenna array", *IEEE Sensors J.*, vol. 9, no. 11, pp. 1557-1566, Nov. 2009

[13] C. Occhiuzzi, S. Caizzone, G. Marrocco, “Passive UHF RFID antennas for sensing applications: principles, methods and classifications”, *IEEE Antennas Propag. Mag.*, vol.55, no. 6, pp. 14-34, Dec. 2013

[14] R. Bhattacharyya, C. Floerkemeier, and S. Sarma, “Towards tag antenna based sensing - an RFID displacement sensor,” *IEEE 2009 Int. Conf. on RFID*, pp. 95 –102, Orlando (USA), Apr. 2009

[15] X. Yi, C. Cho et al., "Wireless strain and crack sensing using a folded patch antenna", *Proc. of European Conf. on Antennas and Propag. (EUCAP) 2012*, Prague (Czech Rep.), Mar. 2012

[16] C. Occhiuzzi, C., Paggi, G. Marrocco, “Passive RFID strain-sensor based on meander-line antennas”, *IEEE Trans. Antennas Propag.*, 59(12), 4836-4840, 2011

[17] S. Caizzone, E. DiGiampaolo, G. Marrocco, “Wireless crack monitoring by stationary phase measurements from coupled RFID tags”, *IEEE Trans. Antennas Propag.* , vol. 62, no. 12, pp. 6412-6419, Dec. 201

[18] S. Manzari, S. Pettinari, G. Marrocco, "Miniaturised wearable UHF-RFID tag with tuning capability," *Electronics Letters* , vol.48, no.21, pp.1325,1326, Oct. 2012

[19] G. Marrocco, "RFID Grids: Part I—electromagnetic theory," *IEEE Trans. Antennas Propag.* , vol.59, no.3, pp.1019-1026, Mar. 2011

[20] J.C. Bolomey, S. Capdevila, L. Jofre, J. Romeu, "Electromagnetic Modeling of RFID-Modulated Scattering Mechanism. Application to Tag Performance Evaluation," Proc. of the IEEE , vol. 98, no. 9, pp. 1555-1569, Sept. 2010

[21] S. Capdevila, L. Jofre, J. Romeu, J.C. Bolomey, "Efficient Parametric Characterization of the Dynamic Performance of an RFID IC", *IEEE Microwave and Wireless Comp. Letters*, vol. 22, no. 8, pp. 436-438, Aug. 2012

[22] J.D. Griffin, G. D. Durgin, "Complete Link Budgets for Backscatter-Radio and RFID Systems", *IEEE Antennas Prop. Mag.*, vol. 51, no. 2, pp. 11-26, Apr. 2009

[23] Datasheet M6e High Performance 4-Port UHF RFID module. Available: www.thingmagic.com

[24] S. Caizzone, G. Marrocco, "RFID Grids: Part II—experimentations," *IEEE Trans. Antennas Propag.* , vol.59, no.8, Aug. 2011